博　士　論　文

Immunocytochemical assessment of cell differentiation of podoplanin-positive osteoblasts into osteocytes in murine bone

（podoplanin 陽性骨芽細胞および骨細胞における組織化学的検索）

平成３１年３月申請

北海道大学

大学院歯学研究科口腔医学専攻

永　井　伯　弥

Immunocytochemical assessment of cell differentiation of podoplanin-positive osteoblasts into osteocytes in murine bone

Tomoya Nagai

Oral Functional Prosthodontics, Graduate School of Dental Medicine, Hokkaido University, Sapporo, Japan

Running title: *Differentiation of podoplanin-positive osteoblasts*

¶Corresponding Author

Tomoya Nagai

Oral Functional Prosthodontics,

Graduate School of Dental Medicine,

Hokkaido University

Kita 13, Nishi 7, Kita-Ku, Sapporo, Hokkaido, 060-8586, Japan

Tel/fax: +81-11-706-4226

E-mail: tnagai@den.hokudai.ac.jp

Abstract

Osteoblastic differentiation into osteocytes is regulated in a temporospatial manner. It is difficult to identify which of osteoblasts are at the verge of differentiating into osteocytes; however, podoplanin reportedly localizes to osteoblasts/osteocytes at the verge of differentiating or right after embedding in the bone matrix. In this study, therefore, we attempted to examine the biological function of podoplanin for osteoblastic differentiation into osteocytes. Podoplanin-reactive osteoblasts show dynamic rearrangement of actin filament distribution and show their assembly along the cell membranes and the basal region of the cytoplasmic processes, whereas osteoblasts with little podoplanin immunoreactivity revealed well-developed stress fibers inside the cells. In the metaphysis (the bone remodeling area), CD44-positive osteoclasts were close to or in contact with podoplanin-reactive osteoblasts showing immunoreactivity of phosphorylated ezrin, an ERM family member associated with actin filament arrangement. Therefore, CD44-positive osteoclasts may participate in the differentiation of podoplanin-positive/phosphorylated ezrin-reactive osteoblasts into osteocytes. Immunoblotting analysis using calvariae from neonatal mice demonstrated increased phosphorylated ezrin when exogenous CD44 was administered. On the endosteal surfaces of cortical bones (a modeling area), bone podoplanin-positive osteoblasts were uniformly localized at certain intervals. Although there was no contact with CD44-positive cells, several osteoblasts showed the immunoreactivities of podoplanin and phosphorylated ezrin. Therefore, unlike femoral trabecules, molecules other than CD44 may transduce the podoplanin/EMR family signaling in preparation for osteocytic differentiation in the cortical bone. Taken together, the interplay between podoplanin and CD44 appears to be, at least in part, associated with ezrin phosphorylation and the subsequent actin rearrangement as well as the facilitation of osteoblastic differentiation into osteocytes in metaphyseal trabecules; however, it does not seem to be associated with the cortical bone.

272 words

Key words: *osteoblast, osteocyte, podoplanin, EMR family, CD44*

Introduction

Osteocytes are the most abundant cells in bone and are connected with bone-covering osteoblasts via thin cytoplasmic processes that pass through the narrow passageway in the bone matrix, *i.e.*, osteocytic canaliculi. Osteocytes can form functional syncytia, by which osteocytic processes are interconnected through gap junctions[1, 2]. Osteocytes and bone-lining osteoblasts can communicate as a group through the osteocytic lacunar-canalicular system (OLCS) [3-6]. The function of OCLS seems to depend on its microscopic arrangement and outreach as the network of connected osteocytic cytoplasmic processes represents the functional area of OLCS. Osteocytic cytoplasmic processes of OLCS are geometrically well-arranged and connected among themselves in mature compact bones but not in immature woven bones[7-10]. The regularly distributed osteocytes and their cytoplasmic processes of OLCS in mature bone suggest the existence of its biological function, suggesting its capability of molecular transport[6, 9, 10], mechanosensing[11], repairing of load-related microdamages[12], targeted bone remodeling[13-15], and bone remodeling adapted to mechanical stresses[16]. Thus, the regularly distributed cytoplasmic processes and osteocytes may be essential for executing their functions in mature bone[7, 9, 10].

To enable geometrically well-arranged distribution of OCLS in the mature bone, there must be a cellular mechanism for the temporospatial transition of osteoblasts into osteocytes that localizes osteocytes in an adequate position with a certain interval in the bone matrix. To define the mechanism, it is apparently important to identify the osteoblasts that are on the verge of differentiation into osteocytes as well as those newly-differentiated osteocytes. Podoplanin[17], also referred to as E11[18], gp38[19], OTS-8[20], and T1α[21], is a 38-kDa type I transmembrane glycoprotein which is expressed in early stages of osteocytes[18]. As Palumbo *et al.* previously proposed the term "preosteocyte" to designate committed osteoblasts which reduce their matrix synthesis and enlarge their area of contact with bone[22], podoplanin appears to an adequate marker of the late stage of osteoblasts and preosteocytes[23-25].

Podoplanin has been detected in various normal tissues besides bone, including podocytes in kidney[26, 27], alveolar epithelial type I cells[28], and basal keratinocytes[29], and plays pivotal roles in cell motility[30], cell adhesion[31], elongation of cytoplasmic processes[32], organogenesis[33-35],

epithelial–mesenchymal transition[36], and others. As an indication of its significant functions, podoplanin-deficient mice die before or shortly after birth, exhibiting defects in many organs, including lung organogenesis, cardiac function, and blood–lymph separation[33-35]. Podoplanin molecule can be divided into an extracellular domain, a single transmembrane domain, and a short cytoplasmic tail, which reportedly interacts with the ezrin/moesin/radixin (ERM) family to activate the small GTPase RhoA through its downstream effector kinase ROCK to phosphorylate ERM and consequently influence the rearrangement of actin cytoskeleton[36-38]. In addition, podoplanin could interact with CD44, a hyaluronan receptor of the cell membrane[39], to promote directional cell migration, suggesting its co-operation with podoplanin[40].

Taken together, we herein postulate that binding with CD44 may accelerate podoplanin function on the rearrangement of actin filaments in osteoblasts on the verge of differentiation into osteocytes because the physiological function of podoplanin during osteocyte differentiation still remains unknown. This study was designated to clarify 1) if the regularly arranged distribution of osteocytes is associated with podoplanin molecules, 2) if there would be any difference in the distribution of podoplanin-positive osteocytes between metaphyseal trabecules (remodeling site) and the endosteal surface of the cortical bone (modeling site), and 3) if there would any interaction between podoplanin-positive osteoblasts and CD44-reactive cells. To do so, we examined the immunolocalization of podoplanin-reactive osteoblasts, as well as the possible interaction of CD44-bearing cells *in vivo* by assessing immunohistochemistry and using immunoelectron microscopy.

Materials and Methods

Animals and tissue preparation

Eight-week-old male ICR mice (CLEA Japan Co. Ltd, Tokyo) were used this study (n = 6), and animal experiments were conducted under the Hokkaido University guidelines for animal experimentation (approval No. 15-0041).

Mice were anesthetized with an intraperitoneal injection of sodium pentobarbital and perfused with 4% paraformaldehyde solution diluted in a 0.067M phosphate buffer (pH 7.4) through their left heart ventricle[41, 42]. After perfusion, femora and tibiae were extracted and immersed in the same fixative for 24 h at 4°C. For light microscopic and stimulated emission depletion (STED) observation, the treated femora and tibiae were decalcified with 10% ethylenediamine tetraacetic disodium salt (EDTA-2Na) solution for 2 months before paraffin-embedding or OTC compound embedding for cryostat sections, respectively. Five -micrometer-thick paraffin sections were made parallel to the longitudinal axis of the bone, and all the paraffin sections subjected to the following histochemistry were photographed under a Nikon Eclipse E800 microscope (Nikon Instruments Inc. Tokyo, Japan), and light microscopic images were acquired with a digital camera (Nikon DXM1200C, Nikon). Cryostat sections with 10–20 μm thickness were used for immunofluorescent staining observed under STED observation or pre-embedding method of immunoelectron microscopy.

Double detection of podoplanin and tissue-nonspecific alkaline phosphatase (TNALPase)

Dewaxed paraffin sections were examined for double detection of podoplanin and tissue-nonspecific alkaline phosphatase (TNALPase) envisioned by the deposition of diaminobenzidine tetrahydrochloride (DAB) and enzyme histochemistry of alkaline phosphatase (ALP) using the Azo dye method, respectively[43]. Briefly, the sections were immersed in PBS containing 0.3% H_2O_2 for 30 min to block endogenous peroxidase. To reduce non-specific binding, 1% bovine serum albumin (BSA, Seologicals Proteins Inc. Kankakee, IL) in PBS (1% BSA–PBS) was applied to the sections for 20 min. The sections were then incubated with polyclonal goat IgG against mouse podoplanin (R&D systems Inc., Minneapolis, MN) at a dilution of 1:100 with 1%BSA–PBS at

room temperature (RT) for 2 h. Following several washings in PBS, they were incubated with horseradish peroxidase (HRP)-conjugated rabbit anti-goat IgG (American Qualex Scientific Products, Inc., San Clemente, CA) for 1 h. The sections were subsequently treated with DAB to visualize the immunoreaction of podoplanin. The treated sections were then incubated with rabbit polyclonal antiserum against TNALPase[44] at a dilution of 1:200 with 1%BSA–PBS at RT for 2 h. Following several washings in PBS, they were incubated with ALP-conjugated anti-rabbit IgG (Chemicon International Inc., Temecula, CA) for 1 h. Briefly, the sections were immersed in a mixture of 6 mg of naphthol AS-BI phosphate (Sigma-Aldrich, St. Louis, MO) and 36 mg of fast blue RR salt (Sigma-Aldrich) diluted in 30 mL of 0.05M Tris-HCl buffer (pH 9.0) at RT until blue color indicative of ALP reactivity was visible. The sections were faintly counterstained with methyl green. For negative control experiments, normal goat serum or rabbit serum was used, following the incubation with HRP- or ALP-conjugated secondary antibodies, respectively.

Podoplanin immunoelectron microscopy

Cryostat sections with 10–20 μm were incubated with 1% BSA–PBS and then with goat IgG to mouse podoplanin (R&D systems) at a dilution of 1:100 with 1%BSA–PBS at 4°C overnight. Following PBS washing for 3–4 h, the sections were incubated with HRP-conjugated rabbit anti-goat IgG (American Qualex Scientific Products, Inc.) at RT for 12 h and washed with PBS for 3–4 h. The treated cryostat sections were incubated with a DAB solution for visualizing immunoreactivity. The sections were fixed with a mixture containing 2% paraformaldehyde and 2.5% glutaraldehyde diluted in 0.067M cacodylate buffer (pH 7.4) for 6 h[41, 43], post-fixed in a mixture of 1% osmium tetraoxide for 4 h, dehydrated with ascending concentrations of acetone, and then embedded in epoxy resin (Taab, Berkshire, UK) [46, 47]. Semi-thin sections and ultrathin sections were cut using ultramicrotome (Sorvall MT-5000; Ivan Sorvall, Inc., Norwalk, CT). The ultrathin sections were faintly stained with uranyl acetate and lead citrate before examination under a TEM (Hitachi H-7100 Hitachi Co. Ltd, Tokyo, Japan) at an accelerating voltage of 80 kV.

Double detection of podoplanin/actin filament and podoplanin/CD44

For detection of podoplanin and actin filament, dewaxed paraffin sections were incubated with 1%

BSA–PBS and then with goat anti-mouse podoplanin (R&D systems) at a dilution of 1:100 with 1% BSA–PBS; then, they were incubated with Alexa Fluor 488-conjugated donkey anti-goat IgG (Abcam plc., Cambridge, Cambridgeshire, UK) and then incubated with rhodamine–phalloidin at a dilution of 1:100 with 1%BSA–PBS after washing with PBS. The treated sections were observed under STED (TCS SP8 STED 3X, Leica Microsystems) equipped at the electron microscope laboratory, Research Faculty of Agriculture, Hokkaido University.

For analyzing the immunolocalization of podoplanin and CD44, the histological sections incubated with goat anti-mouse podoplanin (R&D systems), which were visualized with a DAB solution, were reacted with rat anti-CD44 monoclonal antibody (BD Biosciences, Systems & Reagents Inc., San Jose, CA) at a dilution of 1:100 and then incubated with ALP-conjugated anti-rat IgG (Jackson ImmunoResearch Laboratories Inc., Baltimore, PA) for 1 h. Visualization of ALP-conjugated immune complex was performed using red violet LB salt as follows: 6 mg of naphthol AS-BI phosphate (Sigma-Aldrich) and 36 mg of red violet LB salt (Sigma-Aldrich) diluted in 30 mL of 0.05M Tris-HCl buffer (pH 9.0) at RT until red color indicative of alkaline phosphatase activity was visible.

Triple detection of podoplanin/CD44/TRAP (tartrate-resistant acid phosphatase) and triple immunofluorescent staining for podoplanin/CD44/phosphorylated ezrin

For triple detection of podoplanin/CD44/TRAP, immunohistochemistry for CD44 and podoplanin was performed by enzymatic activities of HRP- and ALP-conjugated second antibodies. Subsequently, the enzymatic activity of tartrate-resistant acid phosphatase (TRAP) was examined[43]. Shortly, the sections were incubated in a mixture of 8 mg of naphthol AS-BI phosphate (Sigma-Aldrich), 70 mg of red violet LB salt (Sigma-Aldrich), and 50mM L(+) tartaric acid (0.76 g, Nacalai Tesque, Kyoto, Japan) diluted in 0.1-M sodium acetate buffer (pH 5.0) for 20 min at 37°C.

For triple immunofluorescent staining of podoplanin/CD44/phosphorylated ezrin, the dewaxed paraffin sections were incubated with goat anti-mouse podoplanin (R&D systems) and then reacted with Alexa Fluor 488-conjugated donkey anti-goat IgG (Abcam plc). The treated sections were then incubated with rat anti-CD44 monoclonal antibody (BD Biosciences, Systems & Reagents

Inc) and TRITC-conjugated goat anti-rat IgG (SouthernBiotech, Inc., Birmingham, AL). To avoid nonspecific binding, immunohistochemistry for podoplanin was performed before CD44 detection. Double-stained sections were reacted with rabbit anti-ezrin (phospho Thr567) polyclonal antibody and then with Alexa Flour 647-conjugated goat anti-rabbit IgG (Thermo Fisher Scientific Inc., Waltham, MA). All the sections were counterstained with DAPI and observed under STED.

Immunoblotting of phosphorylated ezrin in CD44-administered calvariae

The calvariae obtained from neonatal mice with no osteoclasts formed yet[48] were extracted and incubated in αMEM medium including 10% fetal calf serum. Total protein was quantified using Pierce BCA Protein Assay Kit (Thermo Fisher Scientific Inc., Waltham, MA, USA) and denatured by boiling at 100°C for 5 min in 5× sample buffer. The same amount of total protein in each sample was separated by 10% Mini-Protean TGX gels (Bio-Rad Laboratories, Inc., Hercules, CA, USA) and electrophoretically transferred onto polyvinylidene difluoride (PVDF) membranes (Bio-Rad Laboratories, Inc., Hercules, CA, USA). After blocking with 4% bovine serum albumin (BSA) (Sigma-Aldrich, St. Louis, MO, USA) in Tris-buffered saline with Tween 20 (TBS-T) for 1 h at room temperature, the membranes were incubated with Ezrin primary antibody (GeneTex, Inc., Irvine, CA, USA) (1: 650) diluted in 4% BSA in TBS-T at 4°C overnight. Thereafter, the membranes were incubated with horseradish peroxidase-conjugated anti-rabbit secondary antibody (Jackson ImmunoReasearch Laboratories, Inc., West Grove, PA, USA) (1: 3000) for 1 h at RT. After washing, the antigen–antibody complexes were visualized with ECL Prime Western Blotting Detection Reagent (GE Healthcare Life Sciences Inc., Chicago, IL, USA), and image capture and analysis were performed using ImageQuant LAS 4000 (GE Healthcare Life Sciences Inc., Chicago, IL, USA).

Results

Immunolocalization of podoplanin in osteoblasts and osteocytes

When double detection of podoplanin and TNALPase was examined, TNALPase-reactive osteoblasts covered the trabecular surfaces of femoral metaphyses, while podoplanin-reactivity was seen in many osteocytes in the superficial layers of the trabecular bone **(Fig. 1A and B)**. Many osteoblasts close to chondro-osseous junction of femora, wherein bone matrix showed little deposition, showed TNALPase-reactivity but not podoplanin-positivity **(Fig. 1C)**. When observing the distant region from the chondro-osseous junction, however, podoplanin immunoreactivity was seen not only in osteocytes just embedded in the bone but also in some osteoblasts on the bone surface **(Fig. 1D)**. At higher resolution, using semi-thin sections, some osteoblasts, the half of which were embedded in the bone matrix, showed podoplanin immunopositivity. Podoplanin immunopositivity could be seen on cell surfaces of such osteoblasts and osteocytes as well as beneath the osteoblasts **(Fig. 2A, See white arrows)**. Immunoelectron microscopy consistently demonstrated podoplanin immunoreactivity on cell membrane of osteoblasts as well as osteocytes embedded in the superficial layer of the bone matrix **(Fig. 2B and C)**. In addition, podoplanin immunoreactivity was localized to the cytoplasmic processes of these osteoblasts and osteocytes. Thus, podoplanin appears to be a hallmark of newly-differentiated osteocytes and of osteoblasts that are ready to or are about to differentiate into osteocytes.

The distribution of actin filaments in podoplanin-reactive osteoblasts

We postulated the possibility that podoplanin-reactive osteoblasts show the different distribution of actin filament inside cytoplasm when compared to podoplanin-negative osteoblasts. Considering this, double staining for podoplanin and actin filaments was examined using STED. Osteoblasts were filled with numerous actin filaments featuring distribution patterns of stress fibers except in the areas of nuclei. Unlike osteoblasts, osteocytes localized actin filaments along cell membranes and basal parts of cytoplasmic processes but scarcely inside the cytoplasm **(Fig. 3A and B)**. Podoplanin-positive osteoblasts being embedded into the bone showed fewer actin

filaments in the cytoplasmic region but localized actin filaments on the cell membrane and cytoplasmic processes, which resembled those seen in osteocytes rather than osteoblasts **(Fig. 3C and D)**. The merged images of podoplanin and actin filaments showed that podoplanin tended to localize where actin filaments accumulated **(Fig. 3E and F)**. This implies that podoplanin-reactive osteoblasts had already modified the intracellular distribution of actin filaments.

Interplay of CD44 and podoplanin in the regions of bone modeling and remodeling

Next, since podoplanin has a binding site for CD44, we examined double detection of CD44 and podoplanin on endosteal surfaces of the cortical bone which showed continuous bone deposition. Podoplanin-reactive osteoblasts were localized with certain intervals on the endosteal surface of the cortical bone **(Fig. 4A and B)**. There was no cell-to-cell contact between CD44-positive cells and podoplanin-reactive osteoblasts. Most CD44-immunoreactive cells were present in the bone marrow region, and there was an intervening preosteoblastic cell layer between bone marrow and mature osteoblasts **(Fig. 4B)**. However, phosphorylated ezrin, which is a mediator for podoplanin-driven reorganization of actin filaments, was co-localized with podoplanin on the cell membrane of the osteoblasts **(Fig. 4C-E)**. Therefore, in the region of bone modeling, *i.e.,* the endosteal surface of the cortical bone, the osteoblastic differentiation into osteocytes does not seem to be associated with CD44; however, podoplanin-derived signaling appears to be transduced via the phosphorylated ezrin.

The femoral metaphyses, the region of bone remodeling, was subjected to triple staining for podoplanin, CD44, and TRAP. As a result, TRAP-positive osteoclasts showed CD44-immunoreactivity and were often in close proximity of podoplanin-reactive osteoblasts **(Fig. 5A and B)**. Some of these podoplanin-positive osteoblasts also possessed CD44. We examined the phosphorylated ezrin to identify which of the CD44-reactive osteoclasts or podoplanin-positive osteoblasts transduce the signaling derived from CD44 or podoplanin. CD44 was seen on both osteoclast and osteoblasts; however, podoplanin-reactive osteoblasts showed phosphorylated ezrin, while the osteoclast did not show phosphorylated ezrin. Taken together, it is likely that osteoblasts are triggered to differentiate into osteocytes after coming in contact with CD44-positive osteoclasts **(See Fig. 5C-F)**.

Increased phosphorylated ezrin when administered with exogenous CD44 in vitro

For providing a clue for CD44-mediated ezrin phosphorylation, we incubated the calvariae obtained from neonatal mice with 0.4 mg of CD44 and examined the immunoblotting of phosphorylated ezrin time-dependently. As shown in **Fig. 6A and B**, although the increased protein expression levels of phosphorylated ezrin were detected in both control calvariae and CD44-treated calvariae at 24–72 h after incubation, this augmentation was induced significantly more in the latter than in the former. The protein expressions of phosphorylated ezrin were 1.7-, 1.7-, and 1.3-fold higher in CD44-treated calvariae than in controls at 24, 48, and 72 h after incubation, respectively **(See Fig. 6C, D)**.

Discussion

Podoplanin is reportedly expressed abundantly in the late stage of osteoblasts and osteocytes just embedded in the bone[18]. However, there are few reports verifying the biological function of podoplanin in osteoblasts on the verge of differentiation into osteocytes. In our study, we assume that the interplay of podoplanin/CD44/phosphorylated ezrin is associated with osteocytic differentiation in trabecular bone as seen in femoral metaphyses, *i.e.,* bone remodeling area. This implicates the participation of CD44-reactive osteoclasts in osteocytic differentiation from bone-covering osteoblasts. In the mature cortical bone formed by osteoblasts' bone deposition in modeling manner, the interaction of podoplanin and CD44 appeared to be independent of osteocytic differentiation. Thus, our study suggests that osteoclasts are related to osteocytic differentiation in the bone remodeling area but not in modeling sites.

Martin-Villar *et al.*[40] reported that the extracellular domain of podoplanin can bind CD44 to promote directional cell migration of squamous cell carcinomas, implying that CD44 is a novel binding partner for podoplanin, and Martin-Villar et al[36] demonstrated that the ezrin and moesin of the ERM family were linked to the intercellular tail of podoplanin. Therefore, histological assessment of the localization of podoplanin, CD44, phosphorylated ezrin, and actin filament distribution seems appropriate for satisfying our aim in bone remodeling areas (femoral metaphyses). Consequently, histological findings that CD44-bearing osteoclasts were in the close proximity of or in contact with podoplanin-reactive/phosphorylated ezrin-positive osteoblasts and the finding of increased phosphorylated ezrin after CD44 administration in calvarial culture appear to be strong evidences for the possibility that osteoclasts are related to osteocytic differentiation. However, we postulate that the interaction of podoplanin and CD44 between osteoblasts and osteoclasts could facilitate or accelerate osteocytic differentiation in bone remodeling areas. It isn't the intrinsic principal events for osteocytic differentiation, because the podoplanin/phosphorylated ezrin-reactive osteoblasts did not make contact with CD44-positive cells in the bone-modeling area (endosteal cortical bone).

We herein discuss the biological advantage of osteoclasts participating in stimulating

osteoblasts to differentiate into osteocytes. During high bone turnover, many osteoclasts resorb the bone matrix, and mature osteoblasts synthesize surplus bone matrix and get immediately embedded in the bone matrix. Therefore, the osteoblastic preparation or transition ready for osteocytic differentiation appears to be accelerated in the circumstances of high bone turnover, and it seems reasonable that osteoclasts facilitate or stimulate osteoblasts to differentiate into osteocytes. Unlike bone remodeling areas, such as femoral metaphyses, in contrast, in the modeling areas (endosteal surfaces of cortical bones), podoplanin-positive osteoblasts were localized at a certain interval; however, CD44-positive cells were distant from these osteoblasts. Therefore, in the cortical bone, molecules other than CD44 may transduce the podoplanin/ERM family signaling to prepare for osteocytic differentiation. In both regions of bone remodeling and modeling, podoplanin/phosphorylated ezrin seems at least partially necessary for actin filament reorganization for osteocytic differentiation. Our hypothesis on the axis of podoplanin/phosphorylated ezrin is consistent with a recent report demonstrating the alteration of the podoplanin–ezrin–cytoskeleton linkage as an important initiation event of the podocyte injury[49].

As shown in our study, podoplanin-positive osteoblasts were evenly localized to the endosteal surface of the cortical bone, suggesting the geometrically well-arranged distribution of osteocytes in the future **(See Fig. 4)**. Podoplanin definitely seems necessary for a well-arranged distribution of osteocytes in the cortical bone. Staines et al.[50] demonstrated that male and female 6-week-old Oc-cre podoplanin$^{flox/flox}$ knock-out mice showed significantly compromised tibial cortical bone micro-architecture and significantly decreased areas of osteocyte processes. In reverse, the overexpression of podoplanin (E11) in osteoblast-like cells led to the formation of long processes, potentially via the activation of the small GTPase RhoA and the influence on the actin cytoskeleton[36-38]. Therefore, podoplanin seems essential for the regularly distributed osteocytes and their cytoplasmic processes of OLCS in mature bones[7, 9, 10] It is necessary for various biological actions of the bone: molecular transport[6, 9, 10], mechanosensing[11], repairing of load-related microdamages[12], targeted bone remodeling[13-15], and bone remodeling adapted to mechanical stresses[16].

The triggers for accelerating podoplanin-driven signaling in osteoblasts to differentiate

into osteocytes remain unknown. We assumed the mechanical stress-bearing cortical bone as one of the candidates because the podoplanin mRNA (E11 mRNA) expression in osteocytes is up-regulated in response to mechanical stress *in vivo*[25], suggesting a key role for E11 in regulating the cytoskeletal changes associated with process formation and elongation. However, this is still an assumption, and it is necessary for further examination to acquire more information on these issues.

Acknowledgement

We thank the members of the Electron Microscope Laboratory, Research Faculty of Agriculture, Hokkaido University for their technical support.

References

1. Donahue HJ, Li Z, Zhou Z, Yellowley CE: Differentiation of human fetal osteoblastic cells and gap junctional intercellular communication. Am J Physiol Cell Physiol 278:C315-322, 1998.

2. Shapiro F: Variable conformation of GAP junctions linking bone cells: a transmission electron microscopic study of linear, stacked linear, curvilinear, oval, and annular junctions. Calcif Tissue Int 61:285-293, 1997.

3. Amizuka N, Hasegawa T, Oda K, Luiz de Freitas PH, Hoshi K, Li M, Ozawa H: Histology of epiphyseal cartilage calcification and endochondral ossification. Front Biosci (Elite Ed) 1;4:2085-2100, 2012.

4. Hongo H, Hasegawa T, Sasaki M, Suzuki R, Yamada T, Shimoji S, Yamamoto T, Amizuka N: Bone-Orchestrating Cells, Osteocytes. Hokkaido Journal of Dental Science. 32:93-103, 2012.

5. Knothe Tate ML, Niederer P, Knothe U: In vivo tracer transport through the lacunocanalicular system of rat bone in an environment devoid of mechanical loading. Bone 22:107-117, 1998.

6. Knothe Tate ML, Adamson JR, Tami AE, Bauer TW: The osteocyte. Int J Biochem Cell Biol 36:1-8, 2004

7. Hasegawa T, Amizuka N, Yamada T, Liu Z, Miyamoto Y, Yamamoto T, Sasaki M, Hongo H, Suzuki R, de Freitas PH, Yamamoto T, Oda K, Li M: Sclerostin is differently immunolocalized in metaphyseal trabecules and cortical bones of mouse tibiae. Biomed Res 34:153-159, 2013.

8. Hirose S, Li M, Kojima T, de Freitas PH, Ubaidus S, Oda K, Saito C, Amizuka N: A histological assessment on the distribution of the osteocytic lacunar canalicular system using silver staining. J Bone Miner Metab 25:374-382, 2007.

9. Sasaki M, Hongo H, Hasegawa T, Suzuki R, Liu Z, Freitas PHL, Yamada T, Oda K, Yamamoto T, Li M, Totsuka Y, Amizuka N: Morphological aspects of the biological function of the osteocytic lacunar canalicular system and of osteocyte-derived factors. Oral Science International 9:1-8, 2012.

10. Ubaidus S, Li M, Sultana S, de Freitas PH, Oda K, Maeda T, Takagi R, Amizuka N: FGF23 is mainly synthesized by osteocytes in the regularly distributed osteocytic lacunar canalicular system established after physiological bone remodeling. J Electron Microsc (Tokyo) 58:381-

392, 2009.

11. Burger EH, Klein-Nulend J: Mechanotransduction in bone--role of the lacuno-canalicular network. FASEB J 13 Suppl:S101-112, 1999.

12. Mori S, Burr DB: Increased intracortical remodeling following fatigue damage. Bone 14:103-109, 1993.

13. Burr DB: Targeted and nontargeted remodeling. Bone 30:2-4, 2002.

14. Frost HM: Tetracycline-based histological analysis of bone remodeling. Calcif Tissue Res 3:211-237, 1969.

15. Hazenberg JG, Freeley M, Foran E, Lee TC, Taylor D. Microdamage: a cell transducing mechanism based on ruptured osteocyte processes. J Biomech 39:2096-2103, 2006.

16. Huiskes R, Ruimerman R, van Lenthe GH, Janssen JD: Effects of mechanical forces on maintenance and adaptation of form in trabecular bone. Nature 405:704-706, 2000.

17. Breiteneder-Geleff S, Matsui K, Soleiman A, Meraner P, Poczewski H, Kalt R, Schaffner G, Kerjaschki D: Podoplanin, novel 43-kd membrane protein of glomerular epithelial cells, is down-regulated in puromycin nephrosis. Am J Pathol 151:1141-1152, 1997.

18. Wetterwald A, Hoffstetter W, Cecchini MG, Lanske B, Wagner C, Fleisch H, Atkinson M: Characterization and cloning of the E11 antigen, a marker expressed by rat osteoblasts and osteocytes. Bone 18:125-132, 1997.

19. Farr AG, Berry ML, Kim A, Nelson AJ, Welch MP, Aruffo A: Characterization and cloning of a novel glycoprotein expressed by stromal cells in T-dependent areas of peripheral lymphoid tissues. J Exp Med 176:1477-1482, 1992.

20. Nose K, Saito H, Kuroki T: Isolation of a gene sequence induced later by tumor-promoting 12-O-tettradecanoylphorbor-13-acetate in mouse osteoblastic cell (MC3T3-E1) and expressed constituently in ras transformed cells. Cell Growth Differ 1:511-518, 1990.

21. Williams MC, Cao Y, Hinds A, Rishi AK, Wetterwald A: T1 alpha protein is developmentally regulated and expressed by alveolar type I cells, choroid plexus, and ciliary epithelia of adult rats. Am J Respir Cell Mol Biol 14:577-585, 1996.

22. Palumbo C, Palazzini S, Zaffe D, Marotti G: Osteocyte differentiation in the tibia of a newborn rabbit: An ultrastructural study of the formation of cytoplasmic processes. Acta Anat 137:350-358, 1990.

23. Nefussi JR, Sautier JM, Nicolas V, Forest N: How osteoblasts become osteocytes: a decreasing matrix forming process. J Biol Buccale 19:75-82, 1991.

24. Barragan-Adjemian C, Nicolella D, Dusevich V, Dallas MR, Eick JD, Bonewald LF: Mechanism by which MLO-A5 late osteoblasts/early osteocytes mineralize in culture: similarities with mineralization of lamellar bone. Calcif Tissue Int 79:340-353, 2006.

25. Zhang K, Barragan-Adjemian C, Ye L, Kotha S, Dallas M, Lu Y, Zhao S, Harris M, Harris SE, Feng JQ, Bonewald LF: E11/gp38 selective expression in osteocytes: regulation by mechanical strain and role in dendrite elongation. Mol Cell Biol 26:4539-4552, 2006.

26. Matsui K, Breiteneder-Geleff S, Soleiman A, Kowalski H, Kerjaschki D: Podoplanin, a novel 43-kDa membrane protein, controls the shape of podocytes. Nephrol Dial Transplant 14(Suppl):9-11, 1999.

27. Breiteneder-Geleff S, Matsui K, Soleiman A, Meraner P, Poczewski H, Kalt R, Schaffner G, Kerjaschki D: Podoplanin, novel 43-kd membrane protein of glomerular epithelial cells, is down-regulated in puromycin nephrosis. Am J Pathol 151:1141-4152, 1997.

28. Vanderbilt JN, Dobbs LG: Characterization of the gene and promoter for RTI40, a differentiation marker of type I alveolar epithelial cells. Am J Respir Cell Mol Biol 19:662-671, 1998.

29. Schacht V, Dadras SS, Johnson LA, Jackson DG, Hong YK, Detmar M: Up-regulation of the lymphatic marker podoplanin, a mucin-type transmembrane glycoprotein, in human squamous cell carcinomas and germ cell tumors. Am J Pathol 166:913-921, 2005.

30. Krishnan H, Ochoa-Alvarez JA, Shen Y, Nevel E, Lakshminarayanan M, Williams MC, Ramirez MI, Miller WT, Goldberg GS: Serines in the intracellular tail of podoplanin (PDPN) regulate cell motility. J Biol Chem 288:12215-12221, 2013.

31. Tsuneki M, Yamazaki M, Maruyama S, Cheng J, Saku T: Podoplanin-mediated cell adhesion through extracellular matrix in oral squamous cell carcinoma. Lab Invest 93:921-932, 2013.

32. Costa YF, Tjioe KC, Nonogaki S, Soares FA, Lauris JR, Oliveira DT: Are podoplanin and ezrin

involved in the invasion process of the ameloblastomas? Eur J Histochem 59:2451, 2015.

33. Ramirez MI, Millien G, Hinds A, Cao Y, Seldin DC, Williams MC: T1alpha, a lung type I cell differentiation gene, is required for normal lung cell proliferation and alveolus formation at birth. Dev Biol 256:61-72, 2003.

34. Schacht V, Ramirez MI, Hong YK, Hirakawa S, Feng D, Harvey N, Williams M, Dvorak AM, Dvorak HF, Oliver G, Detmar M: T1alpha/podoplanin deficiency disrupts normal lymphatic vasculature formation and causes lymphedema. EMBO J 22:3546-3556, 2003.

35. Mahtab EA, Vicente-Steijn R, Hahurij ND, Jongbloed MR, Wisse LJ, DeRuiter MC, Uhrin P, Zaujec J, Binder BR, Schalij MJ, Poelmann RE, Gittenberger-de Groot AC: Podoplanin deficient mice show a RhoA-related hypoplasia of the sinus venosus myocardium including the sinoatrial node. Dev Dyn 238:183-193, 2009.

36. Martín-Villar E, Megías D, Castel S, Yurrita MM, Vilaró S, Quintanilla M: Podoplanin binds ERM proteins to activate RhoA and promote epithelial-mesenchymal transition. J Cell Sci 119:4541-4553, 2006.

37. Sprague SM, Popovtzer MM, Dranitzki-Elhalel M, Wald H: Parathyroid hormone-induced calcium efflux from cultured bone is mediated by protein kinase C translocation. Am J Physiol 271:F1139-1146, 1996.

38. Martín-Villar E, Borda-d'Agua B, Carrasco-Ramirez P, Renart J, Parsons M, Quintanilla M, Jones GE: Podoplanin mediates ECM degradation by squamous carcinoma cells through control of invadopodia stability. Oncogene 34:4531-4544, 2015.

39. Culty M, Miyake K, Kincade PW, Sikorski E, Butcher EC, Underhill C: The hyaluronate receptor is a member of the CD44 (H-CAM) family of cell surface glycoproteins. J Cell Biol 111:2765-2774, 1990.

40. Martín-Villar E, Fernández-Muñoz B, Parsons M, Yurrita MM, Megías D, Pérez-Gómez E, Jones GE, Quintanilla M: Podoplanin associates with CD44 to promote directional cell migration. Mol Biol Cell 21:4387-4399, 2010.

41. Hasegawa T, Endo T, Tsuchiya E, Kudo A, Shen Zhao, Moritani Y, Abe M, Yamamoto T, Hongo H, Tsuboi K, Yoshida T, Nagai T, Khadiza N, Yokoyama A, Luiz de Freitas PH, Li M, Amizuka N: Biological application of focus ion beam-scanning electron microscopy (FIB-SEM) to the imaging of cartilaginous fibrils and osteoblastic cytoplasmic processes. J Oral

Biosciences 59:55-62, 2017.

42. Hasegawa T, Yamamoto T, Hongo H, Qiu Z, Abe M, Kanesaki T, Tanaka K, Endo T, Freitas PHL, Li M, Amizuka N: Three-dimensional ultrastructure of osteocytes assessed by focused ion beam-scanning electron microscopy (FIB-SEM). Histochem Cell Biol 149:423-432, 2018.

43. Hasegawa T, Amizuka N, Yamada T, Liu Z, Miyamoto Y, Yamamoto T, Sasaki M, Hongo H, Suzuki R, Freitas PHL, Yamamoto T, Oda K, Li M: Sclerostin is differently immunolocalized in metaphyseal trabecules and cortical bones of mouse tibiae. Biomed Res 34:153-159, 2013.

44. Oda K, Amaya Y, Fukushi-Irié M, Kinameri Y, Ohsuye K, Kubota I, Fujimura S, Kobayashi J: A general method for rapid purification of soluble versions of glycosylphosphatidylinositol-anchored proteins expressed in insect cells: an application for human tissue-nonspecific alkaline phosphatase. J Biochem 126:694-699, 1999.

45. Hasegawa T, Yamamoto T, Sakai S, Miyamoto Y, Hongo H, Qiu Z, Abe M, Takeda S, Oda K, Freitas PHL, Li M, Endo K, Amizuka N: Histological effects of the combined administration of eldecalcitol and a parathyroid hormone in the metaphyseal trabeculae of ovariectomized rats. J Histochem Cytochem. In Press.

46. Hasegawa T, Li M, Hara K, Sasaki M, Tabata C, de Freitas PH, Hongo H, Suzuki R, Kobayashi M, Inoue K, Yamamoto T, Oohata N, Oda K, Akiyama Y, Amizuka N: Morphological assessment of bone mineralization in tibial metaphyses of ascorbic acid-deficient ODS rats. Biomed Res 32:259-269, 2011.

47. Yamamoto T, Hasegawa T, Sasaki M, Hongo H, Tsuboi K, Shimizu T, Ota M, Haraguchi M, Takahata M, Oda K, Luiz de Freitas PH, Takakura A, Takao-Kawabata R, Isogai Y, Amizuka N: Frequency of Teriparatide Administration Affects the Histological Pattern of Bone Formation in Young Adult Male Mice. Endocrinology 157:2604-2620, 2016.

48. Amizuka N, Takahashi N, Udagawa N, Suda T, Ozawa H: An Ultrastructural study of cell-cell contact between mouse spleen cells and calvaria-derived osteoblastic cells in a co-culture system for osteoclast formation. Acta Histchem Cytochem 30:351-362, 1997.

49. Suzuki K, Fukusumi Y, Yamazaki M, Kaneko H, Tsuruga K, Tanaka H, Ito E, Matsui K, Kawachi H: Alteration in the podoplanin-ezrin-cytoskeleton linkage is an important initiation event of the podocyte injury in puromycin aminonucleoside nephropathy, a mimic of minimal change nephrotic syndrome. Cell Tissue Res 362:201-213, 2015.

50. Staines KA, Javaheri B, Hohenstein P, Fleming R, Ikpegbu E, Unger E, Hopkinson M, Buttle DJ, Pitsillides AA, Farquharson C: Hypomorphic conditional deletion of E11/Podoplanin reveals a role in osteocyte dendrite elongation. J Cell Physiol 232:3006-3019, 2017.

Figure legends

Figure 1

The distribution of podoplanin and TNALPase in the metaphyseal trabeculae in wild-type femur

TNALPase immunoreactivity was displayed on the osteoblasts located on the bone surface, whereas podoplanin-reactivity was seen in some osteoblasts and many osteocytes presented in the superficial layers of the trabecular bone **(Fig. 1A-B)**. Most osteoblasts proximal to the chondro-osseous junction of femora revealed TNALPase-immunoreactivity but not podoplanin-positivity (arrowheads, **Fig. 1C**). In contrast, at a distant region from the chondro-osseous junction, not only osteocytes but also some osteoblasts expressed both TNALPase-immunoreactivity and podoplanin-positivity (yellow arrows, **Fig. 1D**).

Bars: A: 500 μm; B: 300 μm; C: 20 μm; B: 10 μm

Figure 2

The podoplanin-immunopositivity in semi-thin section and immunoelectron microscopy

On observing the semi-thin sections, podoplanin-positivity was seen on the cell surface of some osteocytes and osteoblasts presented on the half way embedding into bone matrix and as well as close to the osteoblasts (**Fig. 2A**). Under the immunoelectron microscopy of podoplanin, the cell membrane (arrowheads, **Fig. 2B**) and cytoplasmic processes of osteoblasts and osteocytes expressing podoplanin are indicated by black color (**Fig. 2B, C**).

Bars: A: 10 μm; B: 300 μm; C: 4 μm

Figure 3

The distribution of actin filaments and podoplanin in osteoblasts and osteocytes by STED

Osteoblasts located on the bone surface showed that except for the nuclei, the stress fibers consisted of actin filament inside cytoplasm, whereas osteocytes displayed the actin filament along cell membranes and their cytoplasmic processes in the basal site (**Fig. 3A and B**). The distribution of actin filament in podoplanin-positive osteoblasts being embedded into bone matrix revealed on cell membrane and cytoplasmic processes but not the cytoplasm (**Fig. 3C–D**). **Fig. 3E and F** are the merged images of actin filament (**Fig. 3A, B**) and podoplanin (**Fig. 3C, D**).

Bars: A-E: 5 μm

Figure 4

The immunohistochemistry of CD44, podoplanin, and phosphorylated ezrin in the bone modeling region

In the cortical bone, the region of bone modeling where continuous bone deposition occurs, podoplanin-positive osteoblasts were lined at even intervals on the bone surface (**Fig. 4A**). In this region, phosphorylated ezrin was co-localized with podoplanin in the cell membranes of osteoblasts and osteocytes (**Fig. 4C–E**), whereas the podoplanin-positive osteoblasts were not in contact with CD44-positive cells (**Fig. 4B**).

Bars: A, B: 20 μm; C-E: 10 μm

Fig. 5

The immunohistochemistry of CD44, podoplanin, and phosphorylated ezrin in the bone remodeling region

In the femoral metaphyses, the site of bone remodeling, CD44 was expressed in both TRAP-reactive osteoclasts and podoplanin-positive osteoblasts (**Fig. 5A, B**). Furthermore, CD44/TRAP-positive osteoclasts and CD44/podoplanin-positive osteoblasts often presented contiguously in the bone remodeling region (**Fig. 5B**). However, the immunoreactivity to phosphorylated ezrin was observed only in CD44/podoplanin-positive osteoblasts and not in osteoclasts (**Fig 5. C–F**).

Bars: A: 20 μm; B: 10 μm; C-E: 10 μm

Fig. 6

The expression of phosphorylated ezrin protein in control and CD44-treated calvariae

The immunoblotting analysis of phosphorylated ezrin demonstrated the continuously increased protein expression levels in both control and exogenous CD44-treated calvariae (**Fig. 6A, B**). The expression levels of phosphorylated ezrin were 1.7-, 1.7-, and 1.3-fold higher in CD44-treated calvariae than in controls at 24, 48, and 72 h after incubation, respectively (**Fig. 6C, D**).

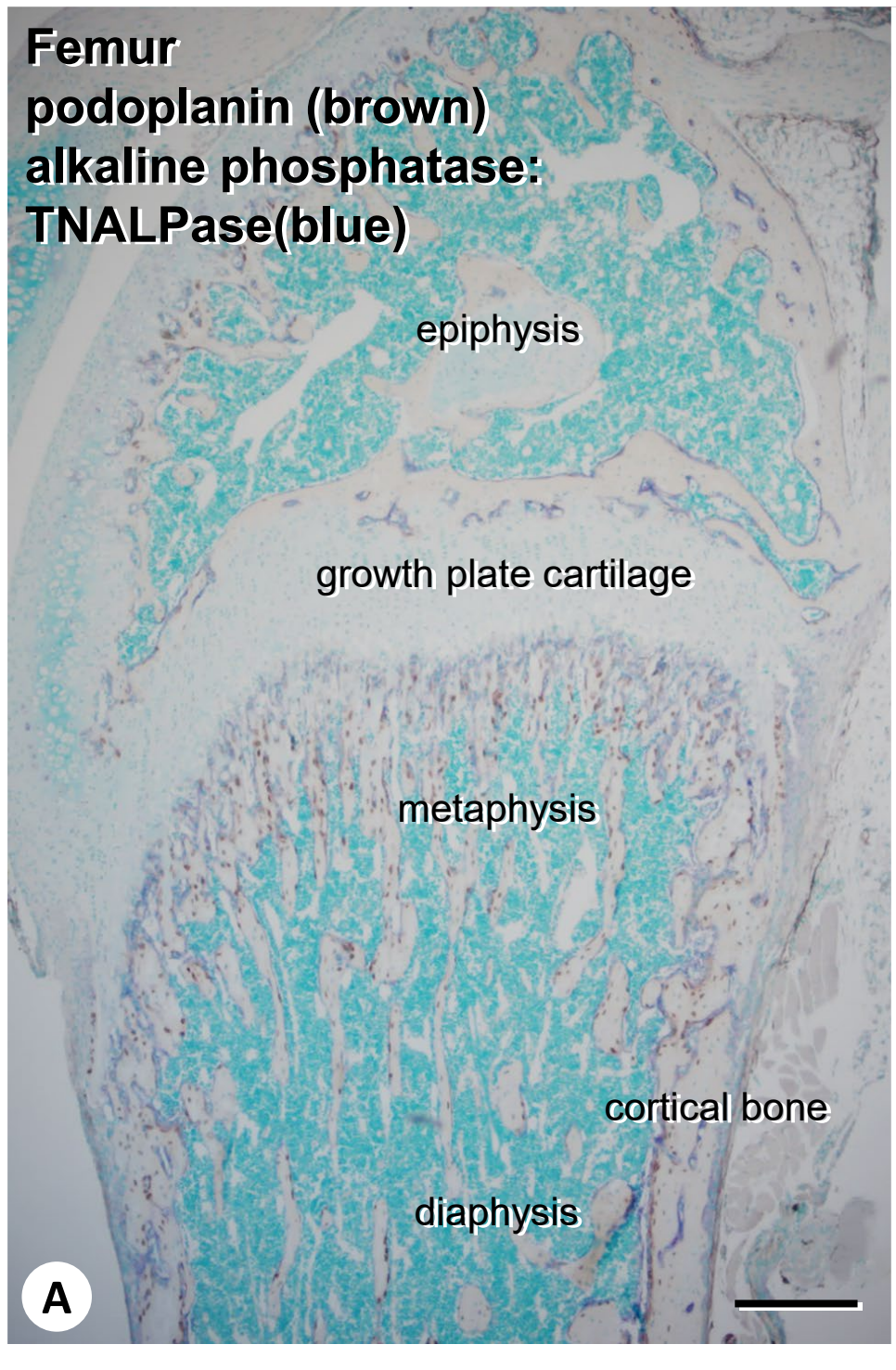
Femur
podoplanin (brown)
alkaline phosphatase:
TNALPase(blue)
epiphysis
growth plate cartilage
metaphysis
cortical bone
diaphysis
A

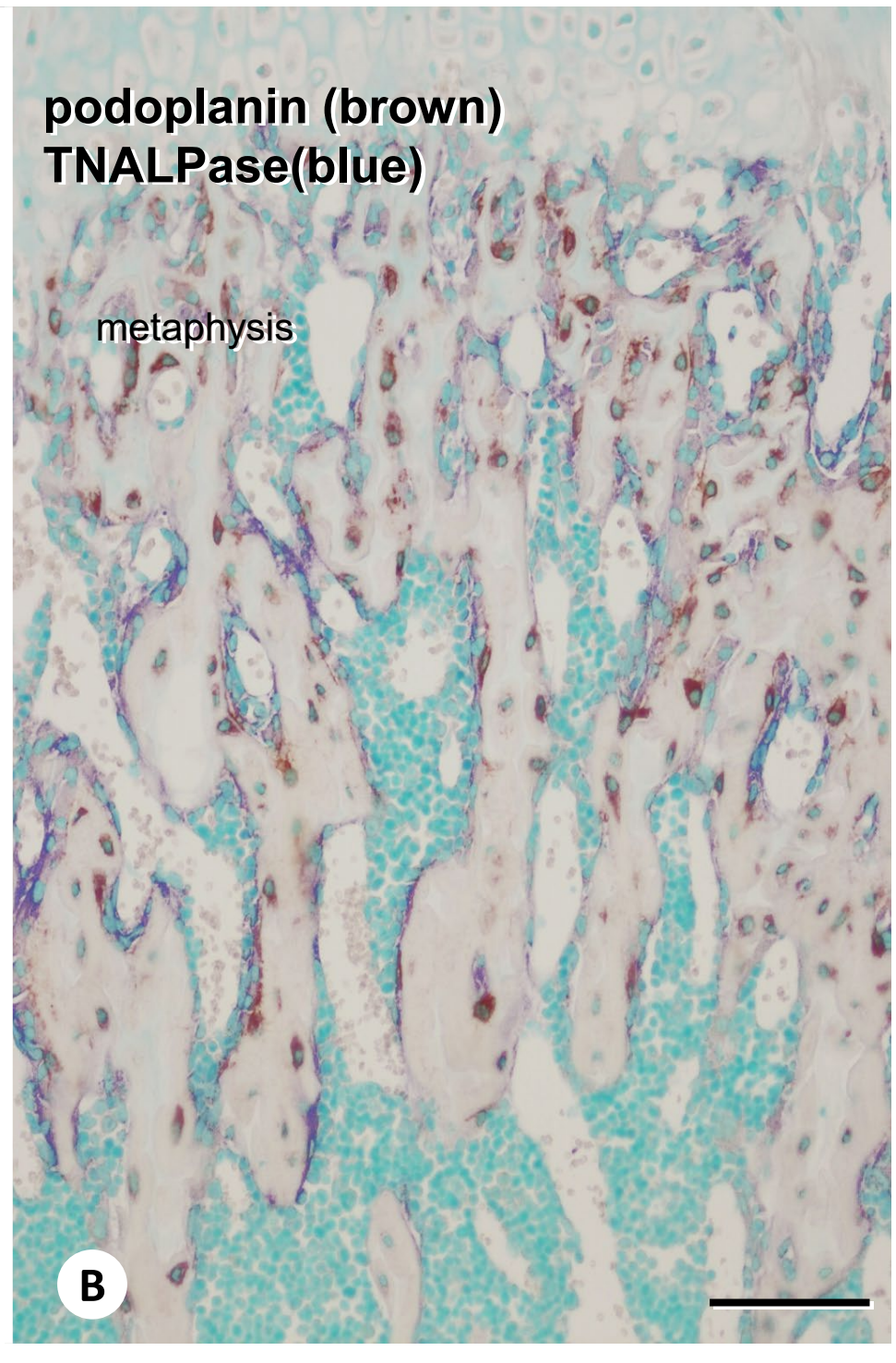
podoplanin (brown)
TNALPase(blue)
metaphysis
B

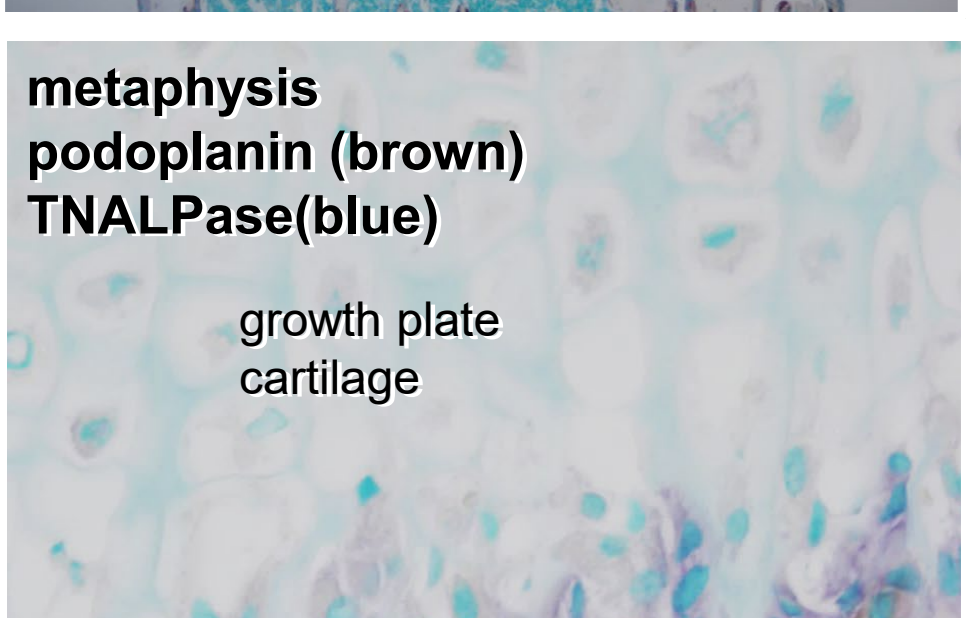
metaphysis
podoplanin (brown)
TNALPase(blue)
growth plate
cartilage
C
Arrowheads: ALP-positive osteoblast
Arrows: podoplanin-reactive osteocyte


podoplanin (brown)
TNALPase(blue)
osteoblast
osteocyte
osteoblast
D

Fig. 1

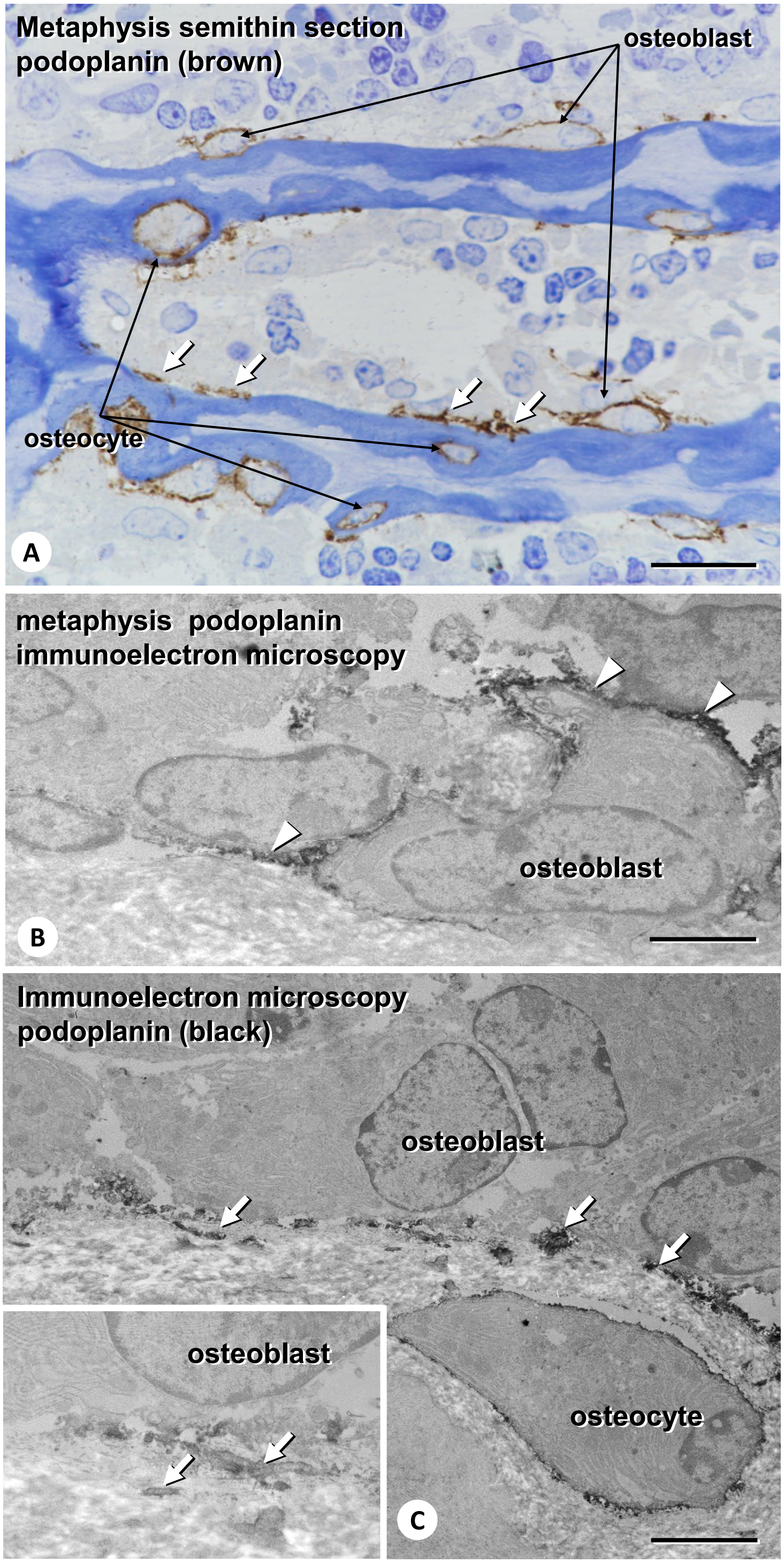
Metaphysis semithin section
podoplanin (brown)
osteoblast
osteocyte
A
metaphysis podoplanin
immunoelectron microscopy
osteoblast
B
Immunoelectron microscopy
podoplanin (black)
osteoblast
osteoblast
osteocyte
C

Fig. 2

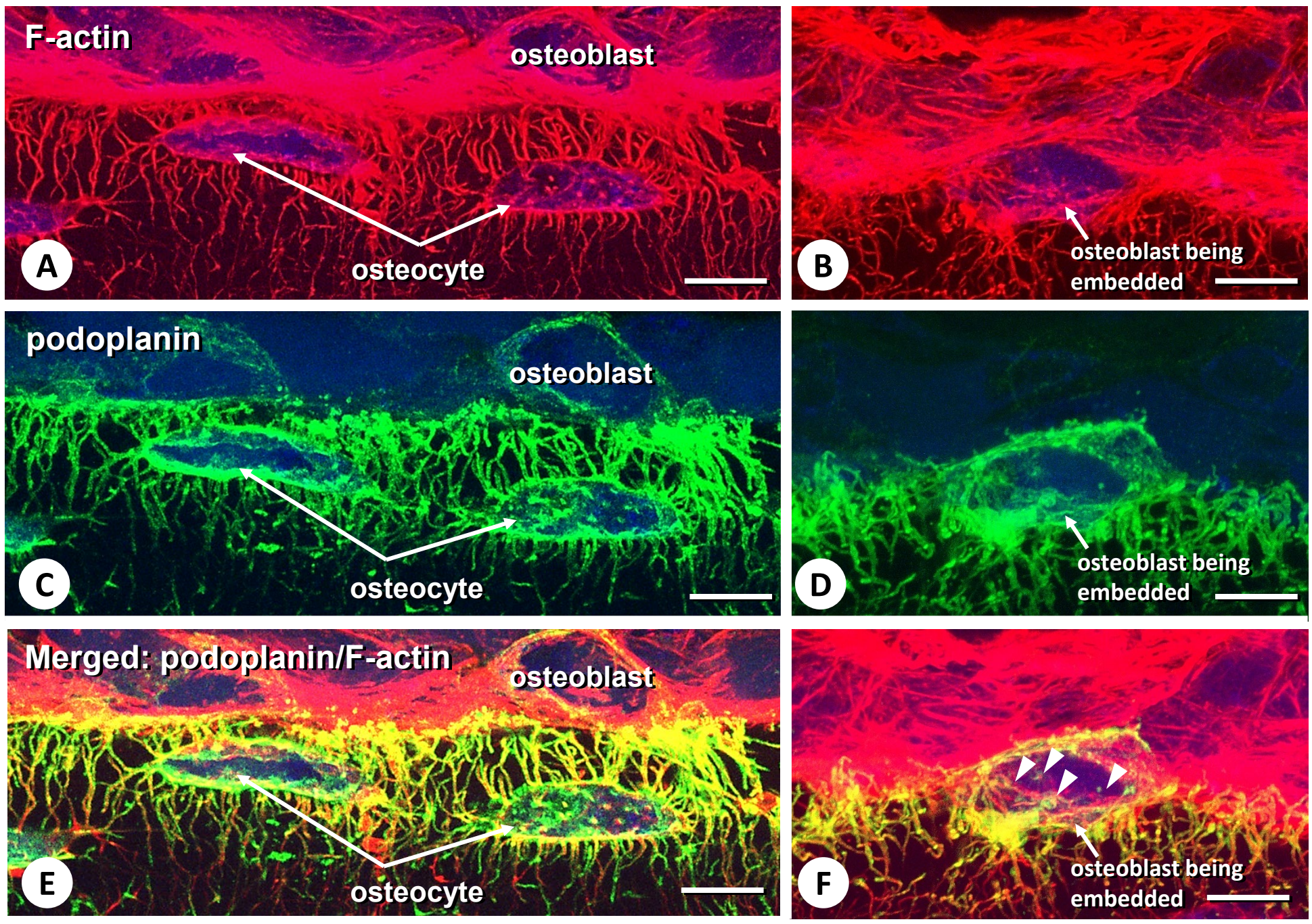
F-actin
osteoblast
osteocyte
A
osteoblast being
embedded
B
podoplanin
osteoblast
osteocyte
C
osteoblast being
embedded
D
Merged: podoplanin/F-actin
osteoblast
osteocyte
E
osteoblast being
embedded
F

Fig. 3

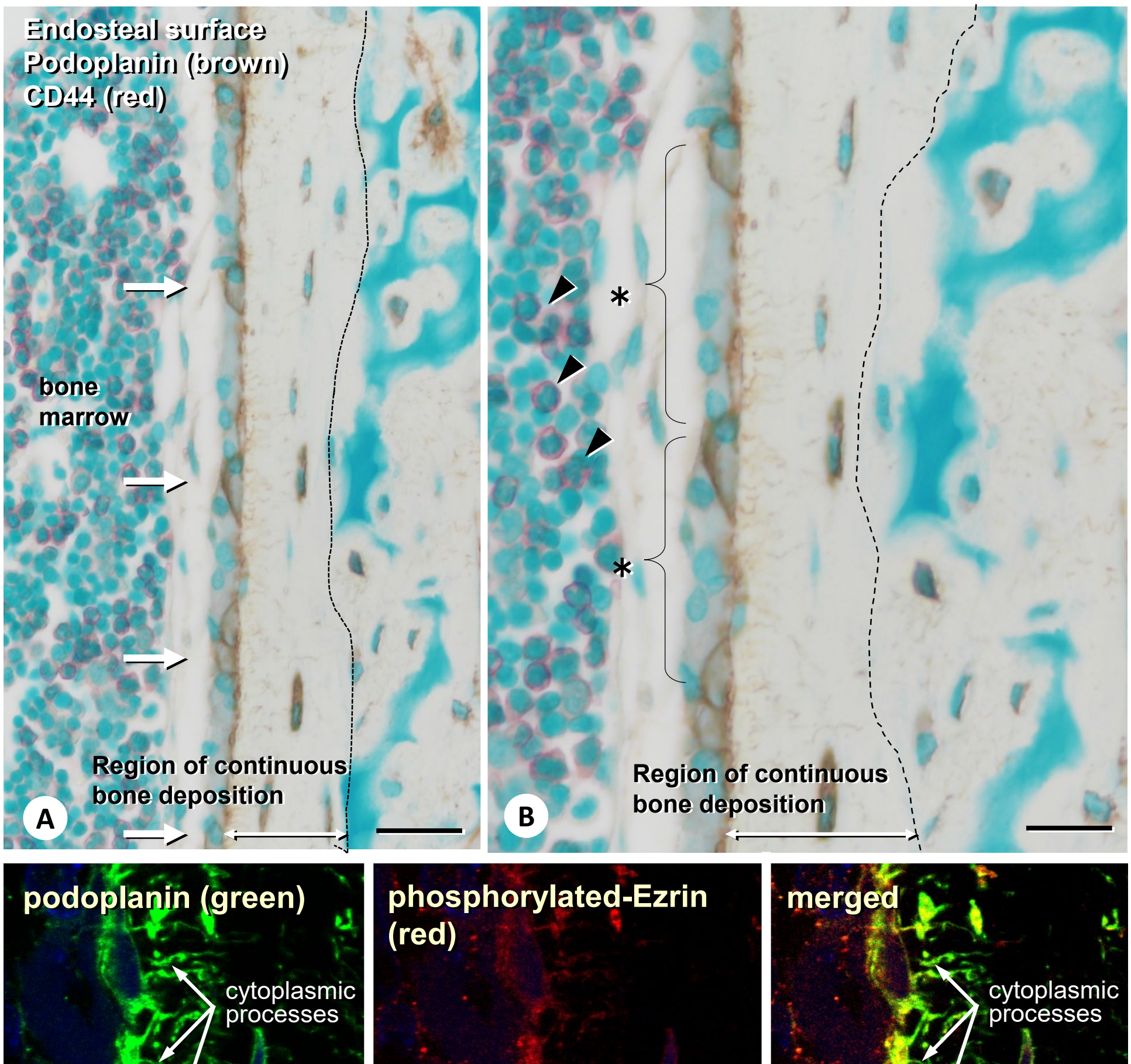
Endosteal surface
Podoplanin (brown)
CD44 (red)
bone marrow
Region of continuous bone deposition
A
*
*
Region of continuous bone deposition
B
podoplanin (green)
cytoplasmic processes
osteoblast
phosphorylated-Ezrin (red)
osteoblast
merged
cytoplasmic processes
osteoblast
osteocyte
Bone matrix
C
osteocyte
Bone matrix
D
osteocyte
Bone matrix
E

Fig. 4

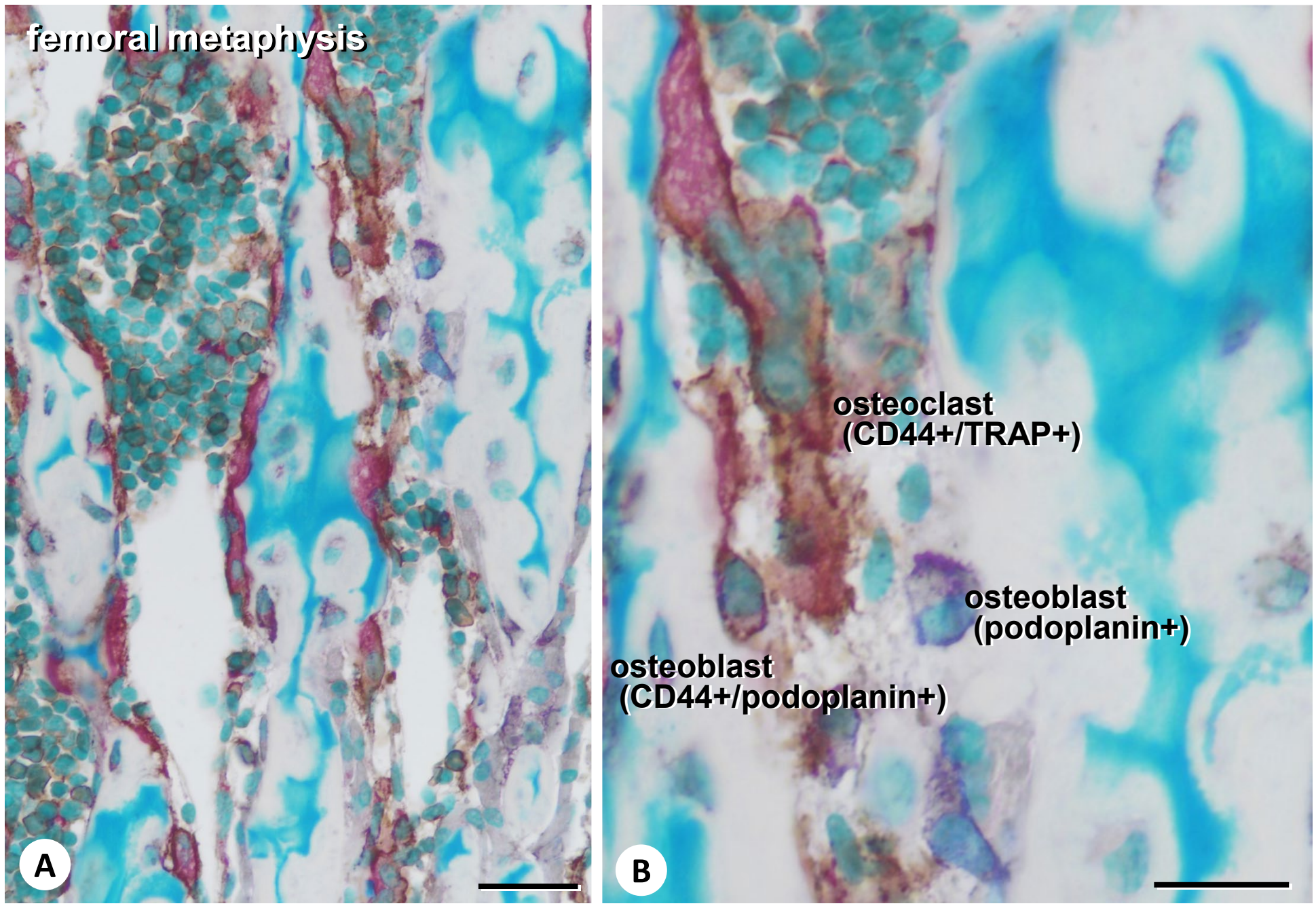
femoral metaphysis
A
osteoclast
(CD44+/TRAP+)
osteoblast
(podoplanin+)
osteoblast
(CD44+/podoplanin+)
B

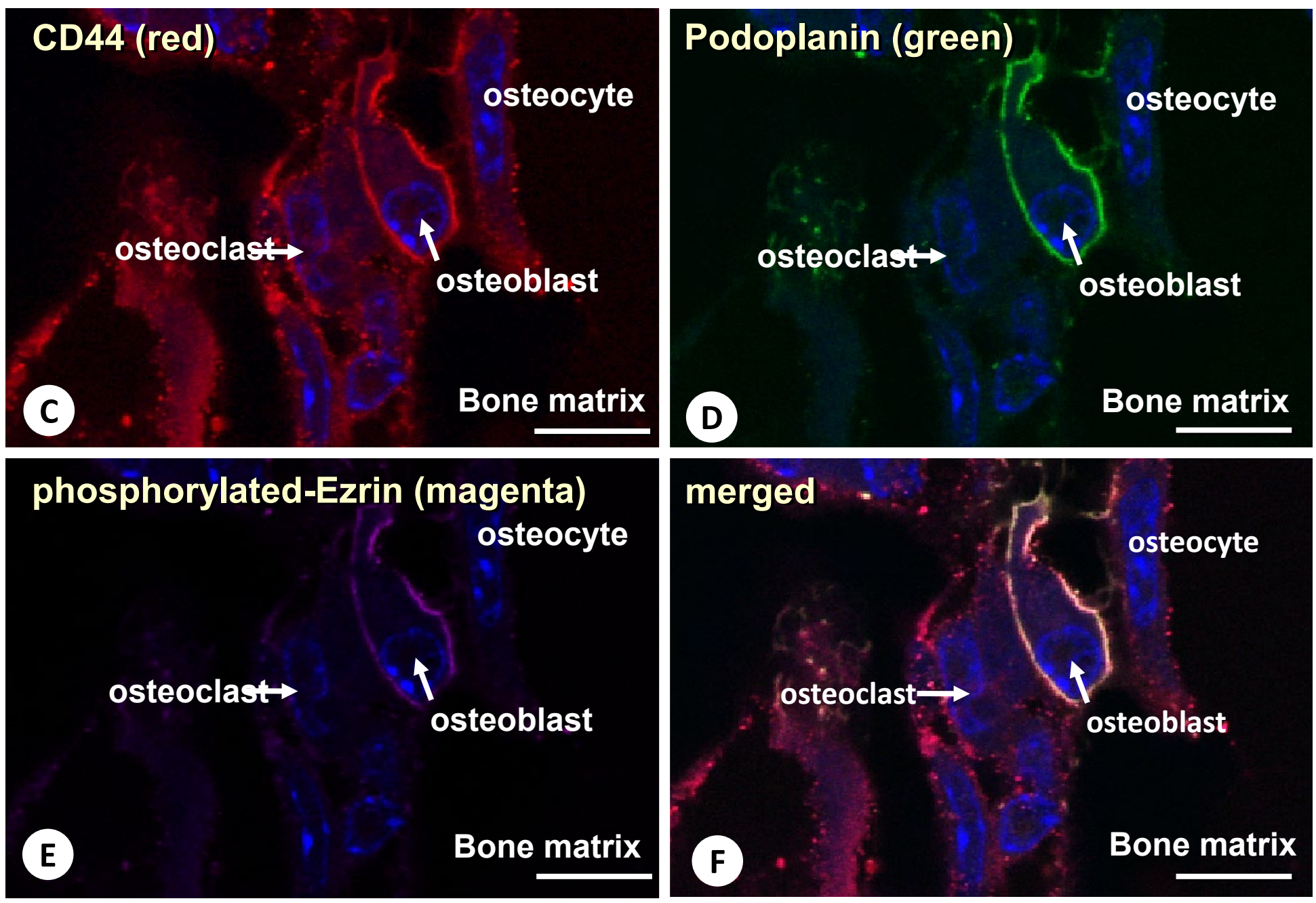
CD44 (red)
osteocyte
osteoclast
osteoblast
Bone matrix
C
Podoplanin (green)
osteocyte
osteoclast
osteoblast
Bone matrix
D
phosphorylated-Ezrin (magenta)
osteocyte
osteoclast
osteoblast
Bone matrix
E
merged
osteocyte
osteoclast
osteoblast
Bone matrix
F

Fig. 5

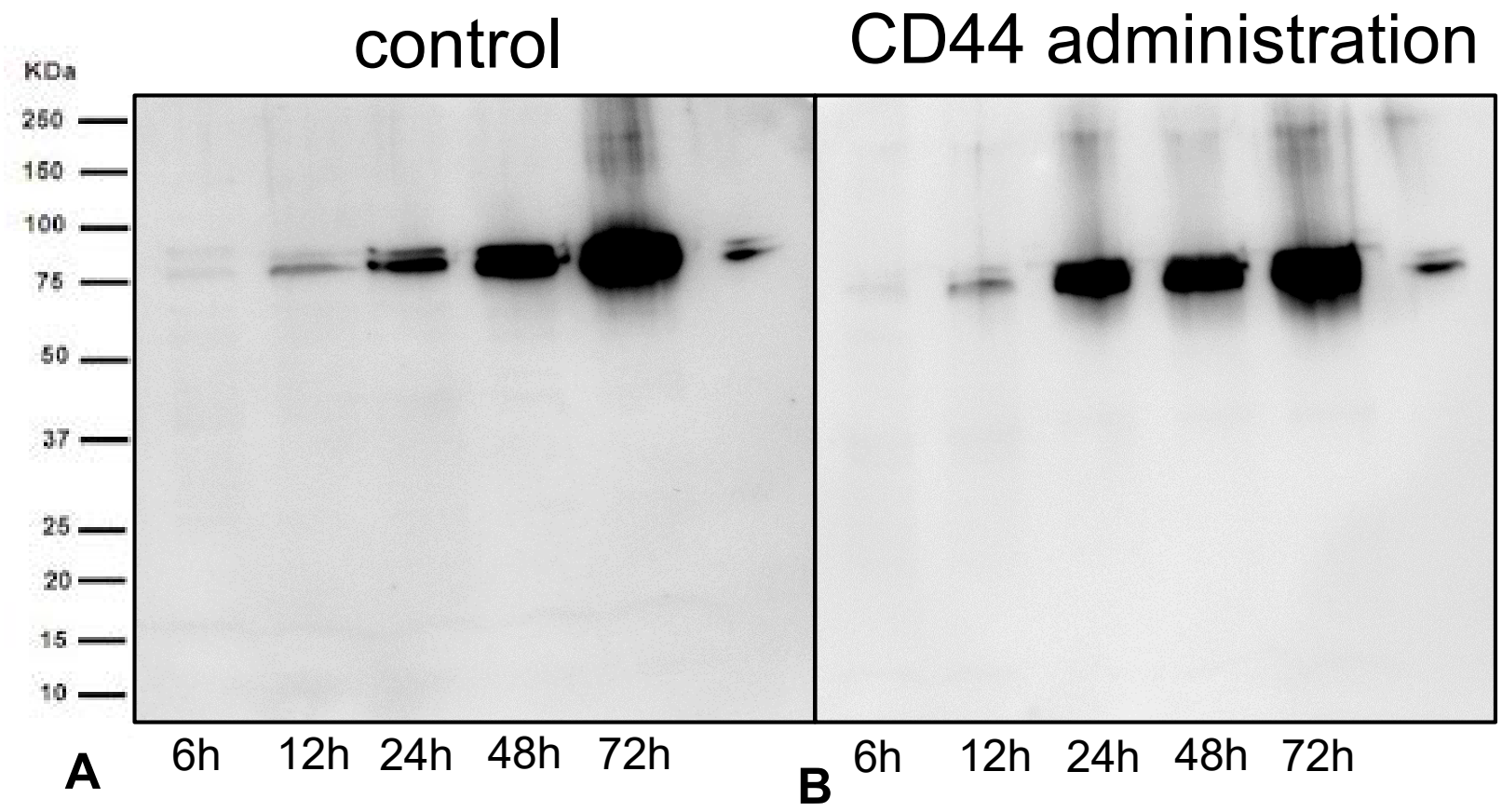
control
CD44 administration
KDa
250
150
100
75
50
37
25
20
15
10
6h
12h
24h
48h
72h
A
B

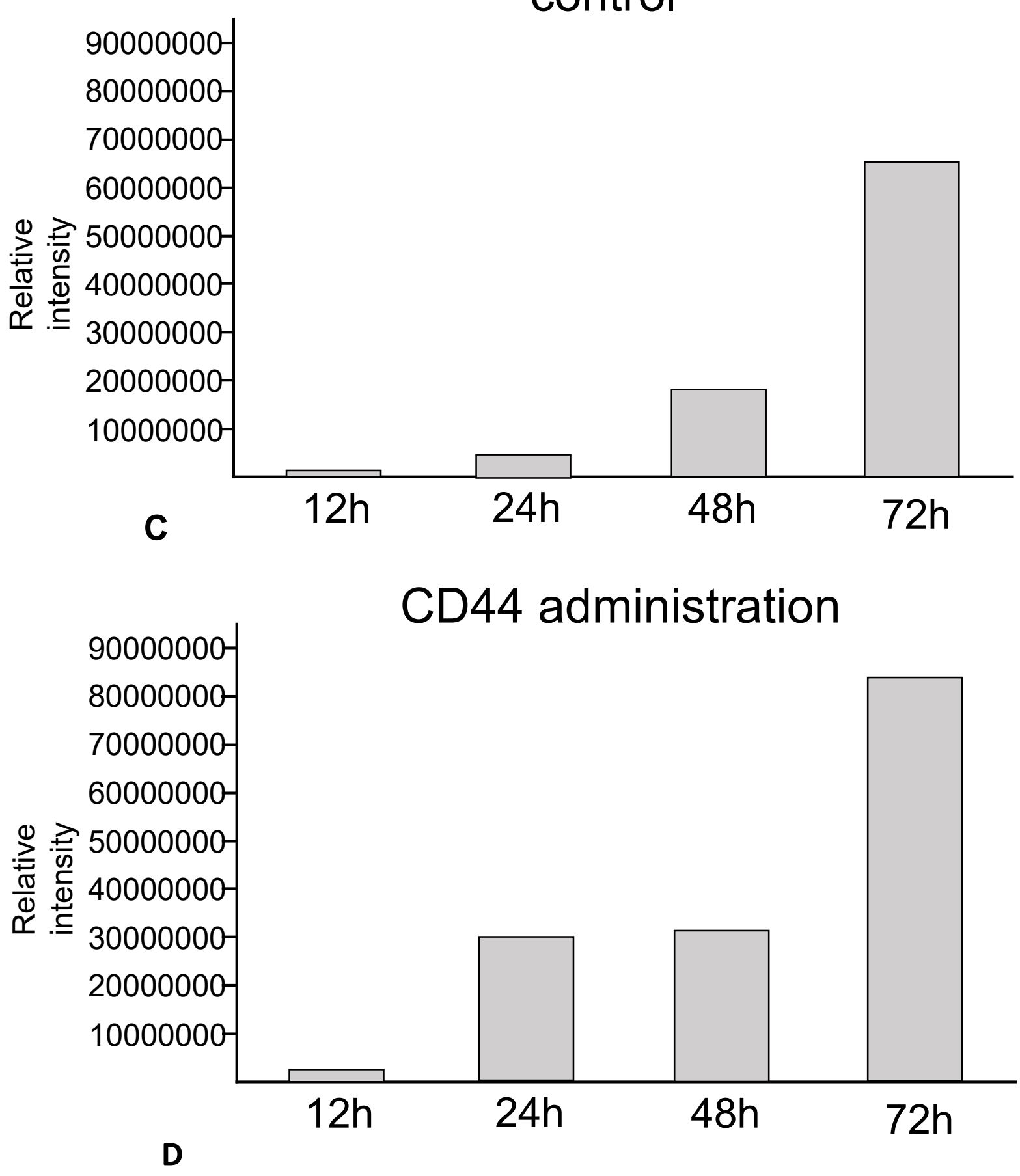
control
Relative intensity
90000000
80000000
70000000
60000000
50000000
40000000
30000000
20000000
10000000
12h
24h
48h
72h
C
CD44 administration
Relative intensity
90000000
80000000
70000000
60000000
50000000
40000000
30000000
20000000
10000000
12h
24h
48h
72h
D

Fig. 6